



**HAL**  
open science

## 1-bit reconfigurable unit-cell based on PIN diodes for transmit-array applications in X-band

Antonio Clemente, Laurent Dussopt, Ronan Sauleau, Potier Patrick, Philippe Pouliguen

► **To cite this version:**

Antonio Clemente, Laurent Dussopt, Ronan Sauleau, Potier Patrick, Philippe Pouliguen. 1-bit reconfigurable unit-cell based on PIN diodes for transmit-array applications in X-band. IEEE Transactions on Antennas and Propagation, 2012, 60 (5), pp.2260 - 2269. 10.1109/TAP.2012.2189716 . cea-03637136

**HAL Id: cea-03637136**

**<https://cea.hal.science/cea-03637136>**

Submitted on 2 May 2022

**HAL** is a multi-disciplinary open access archive for the deposit and dissemination of scientific research documents, whether they are published or not. The documents may come from teaching and research institutions in France or abroad, or from public or private research centers.

L'archive ouverte pluridisciplinaire **HAL**, est destinée au dépôt et à la diffusion de documents scientifiques de niveau recherche, publiés ou non, émanant des établissements d'enseignement et de recherche français ou étrangers, des laboratoires publics ou privés.

# 1-bit Reconfigurable Unit-Cell Based on PIN Diodes for Transmit-Array Applications in X-Band

Antonio Clemente, *Student Member, IEEE*, Laurent Dussopt, *Senior Member, IEEE*, Ronan Sauleau, *Senior Member, IEEE*, Patrick Potier, and Philippe Pouliguen

**Abstract**— An electronically reconfigurable unit-cell with 1-bit phase quantization ( $0^\circ/180^\circ$ ) is proposed for X-band linear polarization transmit-arrays. It consists of two rectangular patch antennas loaded by U- and O-slots and connected by a metallized via hole. The transmission phase is controlled using two PIN diode switches integrated in the O-slot. An equivalent lumped-element circuit model is implemented and compared successfully to full-wave simulations. The numerical results are validated experimentally using an ad-hoc waveguide simulator. The prototype exhibits low insertion loss (1.8 dB) with the same level for both phase states, a broad 3-dB transmission bandwidth (14.7%), a 1-dB compression point of 13-15 dBm and a gain of 5 dBi at 9.75 GHz. The performance and simplicity of the proposed unit-cell make it attractive to build electronically steerable transmit-arrays in X-band.

**Index Terms**— Active unit-cell, active transmit-array antennas, reconfigurable antennas, discrete lens.

## I. INTRODUCTION

LOW-COST and simple electronically-steerable antennas, such as reconfigurable transmit-array antennas (or discrete lenses), are attractive for real-time beam-forming and beam-steering at microwaves and millimeter waves. Automotive radars [1],[2], high data-rate wireless personal and local area networks [3],[4], and high resolution imaging systems are some examples of applications requiring advanced antenna systems.

A transmit-array [5]-[9] typically consists of two planar printed antenna arrays operating in receive ( $R_x$ ) and transmit ( $T_x$ ) modes respectively. The array elements are coupled or interconnected using phase shifters in order to control the phase distribution in the radiating aperture so as to collimate the radiated beam in a given direction ( $T_x$  mode) or to focus the incident energy at the focal point ( $R_x$  mode) similarly as dielectric lens antennas [10]-[12]. They are also attractive for integration onto various platforms since they do not suffer from feed blockage effects (in contrast to reflect-arrays). Finally, their quasi-optical feed eliminates the loss and

complexity of standard beam-forming networks traditionally used in phased arrays.

Quasi-optical power-combining has been an early application of transmit-arrays to mitigate the limited power capabilities of solid-state devices in space or military antenna systems [13],[14]. Since then, beam reconfiguration became the main research focus as many applications require either reconfigurable beamforming, electronic beam-steering or multi-beams capabilities. Beam-steering can be easily achieved by varying the position of the focal source [9],[15],[16]. Likewise, multi-beam capabilities may be achieved using multiple focal sources. Electronic beam-scanning is a more challenging goal as it requires a reconfigurable transmit-array, [similarly to the case of the reflect-arrays \[17\]](#).

Several reconfigurable transmit-arrays have been demonstrated recently using varactor diodes, phase-shifters or MEMS devices [18]-[20]. While these concepts were successfully demonstrated, the experimental antenna efficiency values were severely limited due to the complexity of the array unit-cells which resulted in high insertion losses and/or lack of reliability. In theory, unit-cells with a high phase resolution (i.e. a large number of phase states) are desirable to achieve high beam scanning performances. [However, such cells require many active devices to control the phase states, which results in several limitations \[18\]-\[20\]: higher insertion loss, variation of the insertion loss as a function of the phase state, complexity of the design procedure, integration issues inside a unit-cell whose size is typically in the order of half a wavelength.](#)

Therefore, if power efficiency is a primary concern, a relaxed phase resolution may be chosen at the cost of higher quantization losses. Quantization losses do not correspond to actual power losses but only a reduction of the focusing capabilities of the array, i.e. a lower directivity and aperture efficiency. Our previous work on X-band and V-band transmit-arrays showed that, [as for reflect-arrays \[17\]](#), a 1- to 2-bit phase resolution ( $180^\circ$  and  $90^\circ$  phase steps, respectively) typically results in a quantization loss of 1 to 4 dB [8],[15]. It is interesting to note that a similar trade-off on phase resolution vs. complexity occurs in reflect-array antennas [21],[22]. [We believe that such arrays, with relaxed specifications on side-lobe level, would find applications in the domain of wireless communications such as point-to-point radio links, metropolitan area networks, or satcoms, as well as some low-cost radars for surveillance or traffic monitoring.](#)

We introduce here a new configuration of unit-cell with 1-

---

Manuscript received March 31, 2011, revised September 22, 2011.

A. Clemente and L. Dussopt are with CEA-LETI, Minatex Campus, F38054 Grenoble, France (e-mail: [antonio.clemente@cea.fr](mailto:antonio.clemente@cea.fr), [laurent.dussopt@cea.fr](mailto:laurent.dussopt@cea.fr)).

R. Sauleau is with the Institute of Electronics and Telecommunications of Rennes (IETR), UMR CNRS 6164, University of Rennes 1, F35042, Rennes, France (e-mail: [ronan.sauleau@univ-rennes1.fr](mailto:ronan.sauleau@univ-rennes1.fr)).

P. Potier is with the Direction Générale de l'Armement (DGA), F35174, Bruz cedex, France (e-mail: [patrick.potier@dga.defense.gouv.fr](mailto:patrick.potier@dga.defense.gouv.fr)).

P. Pouliguen is with the Direction Générale de l'Armement (DGA), Strategy Directorate, Office for Advanced Research and Innovation, F92221 Bagneux cedex, France (e-mail: [philippe.pouliguen@dga.defense.gouv.fr](mailto:philippe.pouliguen@dga.defense.gouv.fr)).

bit phase resolution in X-band [23]. It uses only two PIN diodes and a single biasing signal. This design exhibits low insertion loss and a wide transmission bandwidth independent of the phase state. Its operation principle and lumped-element equivalent circuit model are explained in Sections II and III respectively. Simulation results are provided in Section III and validated experimentally in Section IV, which includes also radiation and linearity characterizations. Finally conclusions are drawn in Section V.

## II. 1-BIT UNIT-CELL: LAYOUT AND OPERATION PRINCIPLE

The proposed unit-cell is represented in Fig. 1. It consists of a rectangular patch antenna ( $7.03 \times 8.2 \text{ mm}^2$ ) loaded by a U-slot on one side and a patch antenna of same size loaded by an O-slot on the opposite side. Both patches are connected by a metallized via hole ( $d_v = 0.38 \text{ mm}$ ) located at their center. They are printed on two identical substrates (Rogers RO4003,  $\epsilon_{r,sub} = 3.55$ ,  $\tan\delta = 0.0027$ ,  $h = 1.524 \text{ mm}$ ) separated by a  $18 \text{ }\mu\text{m}$ -thick copper ground plane and are bonded by a RO4403 film ( $\epsilon_{r,film} = 3.38$ ,  $h_b = 0.09 \text{ mm}$ ).

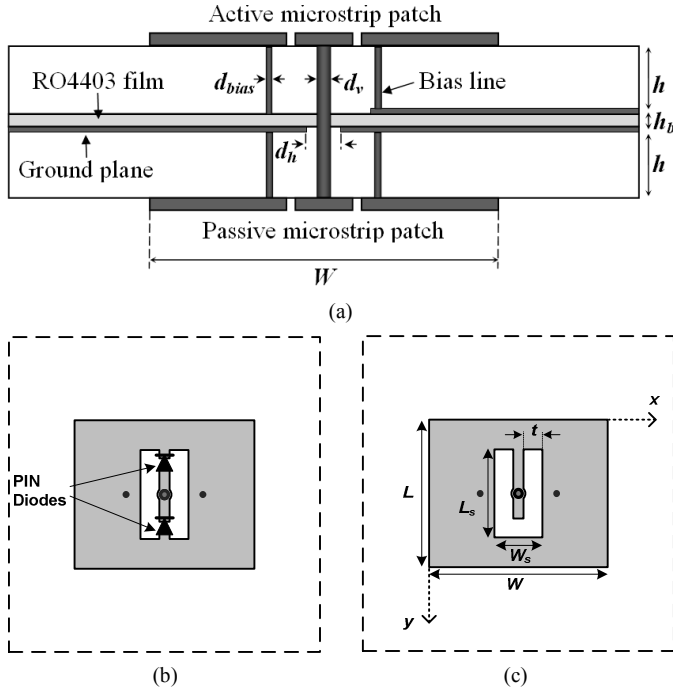


Fig. 1. Geometry of the unit-cell. (a) Cross section view. (b) Active patch with two PIN diodes in the O slot. (c) Passive patch loaded by the U slot. Unit-cell size:  $15 \times 15 \text{ mm}^2$  ( $\lambda_0/2 \times \lambda_0/2$  at 10 GHz).

The U-slot loaded patch (Fig. 1c), referred to as the passive patch in the following, is connected to the ground plane for biasing purposes through two vertical via holes ( $d_{bias} = 0.15 \text{ mm}$ , Fig. 1a); the latter are located along the median line of the patch where a near-zero electric field is expected. Although a single connection is necessary for biasing, a dual connection was preferred to keep symmetry, and thus led to lower cross-polarization levels. Two AlGaAs flip chip PIN diodes [24] are integrated in the O-slot loaded patch (active patch (Fig. 1b)). This patch is connected to a narrow ( $0.21 \text{ mm}$ ) bias line through a vertical connection ( $d_{bias} = 0.15 \text{ mm}$ ) similar to the passive patch. A dummy vertical via hole was also inserted on the opposite side to preserve the symmetry of

the patch antenna. The bias line is very thin and close to the ground plane, so that it does not interact with the patch antenna. This is very important in prevision of the realization of a large transmit-array with many bias lines running in parallel. We have validated by full-wave simulations that the performance of the unit-cell is not modified with at least five bias lines on each side of the unit-cell.

The two PIN diodes are oriented in opposite ways as shown in Fig. 1b, so that they are biased in opposite states when using a single biasing signal. Therefore, the O-slot is always short-circuited at one of its ends and thus resembles to the U-slot of the passive patch. Depending on the bias current sign, the incident field is thus transmitted in phase or with a  $180^\circ$  rotation, resulting a 1-bit differential phase-shift ( $0^\circ/180^\circ$ ).

All geometrical and electrical parameters are summarized in Table I.

TABLE I  
MAIN FEATURES OF THE UNIT-CELL

Parameter	Value
Unit-cell size	$15 \text{ mm} \times 15 \text{ mm}$
Patch size	$L = 7.03 \text{ mm}$ , $W = 8.2 \text{ mm}$
Slot size	$L_s = 3 \text{ mm}$ , $t = 0.9 \text{ mm}$ , $W_s = 2.22 \text{ mm}$
Substrate	Rogers RO4003 ( $\epsilon_{r,sub} = 3.55$ , $\tan\delta = 0.0027$ , $h = 1.524 \text{ mm}$ )
Bonding film	Rogers RO4403 ( $\epsilon_{r,film} = 3.38$ , $h_b = 0.09 \text{ mm}$ )
Connection via	$d_v = 0.38 \text{ mm}$
Ground plane opening	$d_h = 0.6 \text{ mm}$
Bias via	$d_{bias} = 0.15 \text{ mm}$
PIN diodes	MACOM AlGaAs flip chip MA4AGP907

## III. MODELING OF THE UNIT-CELL

### A. PIN diodes: experimental characterization and modeling

A diode has been mounted in series on a coplanar transmission line and measured using coplanar probes (Fig. 2a). A full 2-ports calibration has been applied at the ends of the coplanar line. The electrical parameters of the diode equivalent model (Fig. 2b and 2c) in the *on* and *off* states [24],[25] have been derived by fitting measurements and simulations. The measured reflection and transmission coefficients are represented in amplitude (Fig. 3a) and phase (Fig. 3b), for forward ( $S_{11}^{Fwd}$ ,  $S_{21}^{Fwd}$ ,  $I_{bias} = 10 \text{ mA}$ ) and reverse ( $S_{11}^{Rev}$ ,  $S_{21}^{Rev}$ ,  $V_{bias} = 5 \text{ V}$ ) biasing, respectively.

The series resistance was found to vary from  $8.6 \text{ }\Omega$  to  $3.6 \text{ }\Omega$  as a function of the biasing current in the range 1-10 mA. All simulation results presented in this paper assume a forward bias current of 10 mA. For this bias value, the nominal values of the electrical model ( $Z_{ON}$ ) are  $R_s = 3.6 \text{ }\Omega$ , and  $L_d = 0.05 \text{ nH}$ .

For reverse bias ( $V_{bias} = 5 \text{ V}$ , *off*-state), the electrical model ( $Z_{OFF}$ ) is given by  $C_t = 42 \text{ fF}$ ,  $R_p = 300 \text{ k}\Omega$ ,  $L_d = 0.05 \text{ nH}$ . Additional measurements have shown that these parameters are very stable for a reverse voltage in the range of 1 V and 20 V.

It is important to note that the diodes are mounted on the unit-cell in an anti-parallel configuration as illustrated in Fig. 1b. This means that the *off*-state diode is reverse biased by the forward threshold voltage of the *on*-state diode, which is on the order of 1.22 V. This reverse voltage was found to be

sufficient to guarantee a good isolation.

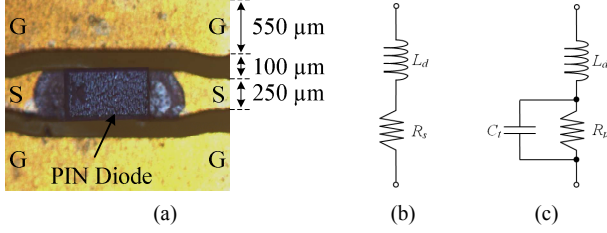
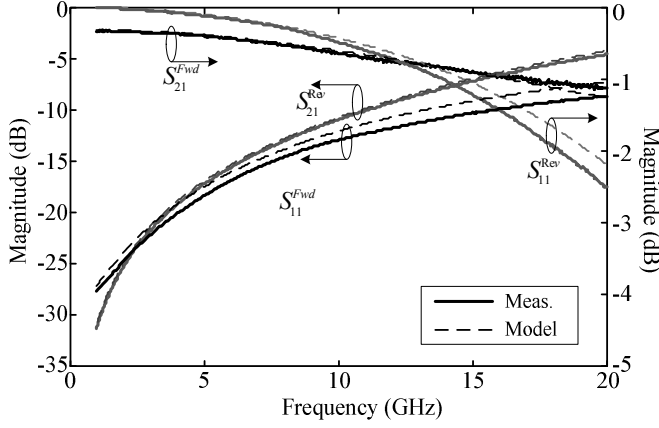
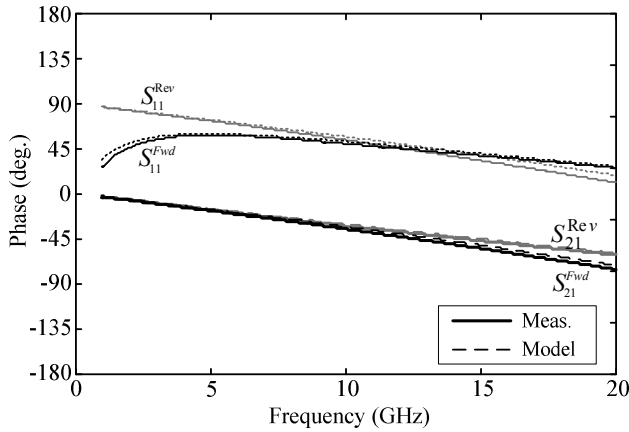


Fig. 2. (a) Fabricated prototype for the experimental characterization of the PIN diodes. Equivalent model of the PIN diode: (b) forward bias ( $Z_{ON}$ ), (c) reverse bias ( $Z_{OFF}$ ).



(a)



(b)

Fig. 3. Measured and modeled  $S$ -parameters of the PIN diodes in the forward ( $I_{bias} = 10$  mA) and reverse ( $V_{bias} = 5$  V) bias states: magnitude (a) and phase (b). Solid line: measurement. Dashed line: electrical model.

### B. Description of the lumped-element electrical model

An equivalent electrical model of the reconfigurable unit-cell is proposed in Fig. 4. In this model, all lumped elements are described analytically and take into account the physical parameters of the structure:

- Each slot-loaded patch is represented by two impedances:  $Z_p^P$  and  $Z_s^P$  for the passive patch, and  $Z_p^A$  and  $Z_s^A$  for the active one. The superscripts  $P$  and  $A$  stand for ‘Passive’ and ‘Active’, while the subscripts  $P$  and  $S$  stand for ‘Patch’ and ‘Slot’.
- Both patches are coupled to input/output  $377 \Omega$  free-space

ports through ideal transformers,

- The PIN diode equivalent circuit ( $Z_{ON}$  and  $Z_{OFF}$ , for forward and reverse bias, respectively) are connected to the active patch. The OFF diode ( $Z_{OFF}$ ) is in parallel with the slot ( $Z_s^A$ ), while the ON diode ( $Z_{ON}$ ) is in series between the active patch and the via connection. As the diodes are integrated on a radiating element, it was found that an additional capacitor ( $C_{pk} = 25$  fF) was necessary to take into account the bulk GaAs body of the diode; this value was extracted from electromagnetic simulations.
- The T-network ( $L_v, C_h, L_v$ ) models the metallized via connecting both patches.

The derivation of these parameters is described in the following section.

### C. Analytical derivation of the lumped elements

U-slot microstrip patch antennas have been investigated in several papers [26],[27]. They exhibit a dual resonance behavior: the first resonance corresponds to the first resonant mode  $TM_{10}$  of the microstrip patch, and the second one is due to the U slot. Their approximate expressions have been derived in [26] and are given below

$$f_1 = \frac{c}{\sqrt{\epsilon_r} \left( \frac{3}{2}L + 3\Delta L + W_s + \frac{1}{2}L_s \right)}, \quad (1a)$$

$$f_2 = \frac{c}{\sqrt{\epsilon_r} \left( \frac{1}{4}L + \frac{W}{2} + \frac{3}{2}\Delta L + \frac{3}{4}L_s - \frac{W_s}{4} + \frac{t}{2} \right)}. \quad (1b)$$

$c$  is the speed of light in vacuum, and the patch length extension  $\Delta L$  is given by

$$\Delta L = 0.412h \frac{(\epsilon_{eff} + 0.300)(W/h + 0.264)}{(\epsilon_{eff} - 0.258)(W/h + 0.813)}, \quad (2)$$

where  $\epsilon_{eff}$  is the effective dielectric constant of the substrate [28]p. 267].

To represent this dual-resonance behavior, the passive and active patches are modeled as a combination of a shunt parallel  $RLC$  resonator ( $Z_p^{P,A} \equiv (R_p^{P,A}, L_p^{P,A}, C_p^{P,A})$ ) and a series complex impedance ( $Z_s^{P,A} = R_s^{P,A} + jX_s^{P,A}$ ) (Fig. 4).  $Z_p^P$  and  $Z_p^A$  are derived using the cavity model for the fundamental  $TM_{10}$  mode [28],[29]

$$Z_p^{P,A} = \left[ \frac{1}{R_p^{P,A}} + j\omega C_p^{P,A} + \frac{1}{j\omega L_p^{P,A}} \right]^{-1}, \quad (3)$$

where

$$C_p^{P,A} = \frac{\epsilon_0 \epsilon_{r,sub} LW}{2h} \cos^{-2} \left( \frac{\pi y_0}{L} \right), \quad (4a)$$

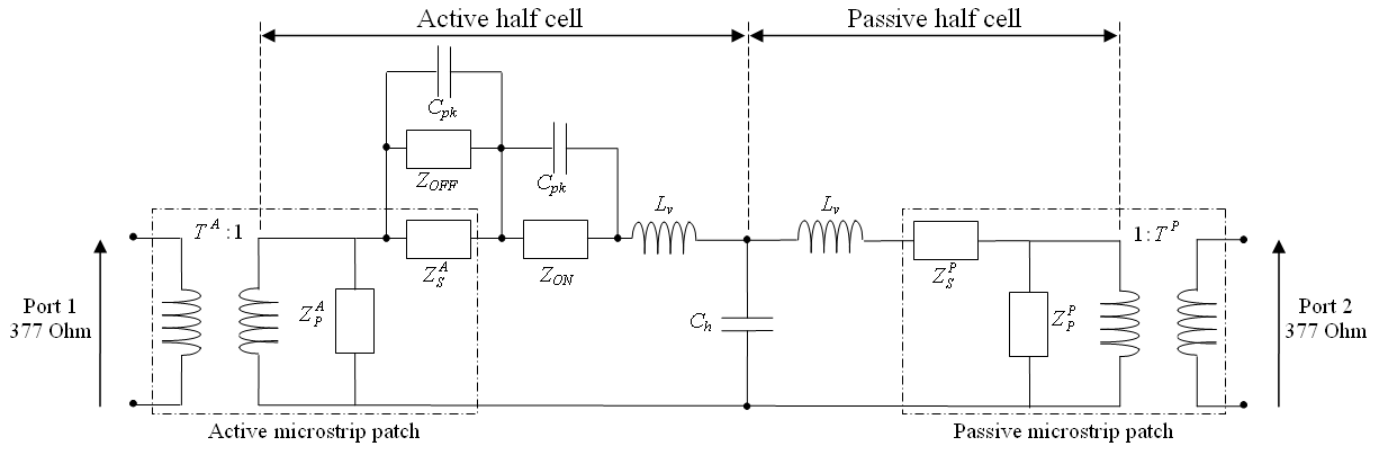


Fig. 4. Lumped-element electrical model of the 1-bit unit-cell.

$$R_p^{P,A} = \frac{Q_l}{C_p^{P,A} 2\pi f_1}, \text{ and} \quad (4b)$$

$$L_p^{P,A} = \frac{1}{C_p^{P,A} (2\pi f_1)^2}. \quad (4c)$$

$Q_l$  is the quality factor due to dielectric, surface wave, and ohmic losses [28]p. 281],[30]p. 853], and  $y_0$  is the distance of the excitation point from the closest radiating edge. In contrast to a standard microstrip patch, the effective position of the excitation point is not well defined here because of the U-slot. It is located somewhere between the vertical via at the center of the patch ( $L/2$ ) and the top of the U-slot ( $(L - L_s)/2$ ). We have found that the value  $y_0 = 0.43L$  was leading to a good fit between the model and the electromagnetic simulations.

The resistance  $R_p^{P,A}$  (Eqn. 4b) corresponds only to the loss in the radiating elements. The radiation resistances are taken into account in the transforming ratio ( $T^{P,A}$ ) of both coupling transformers

$$T^{P,A} = R_r^{P,A} / \eta_0, \quad (5)$$

where  $\eta_0 = 377 \Omega$  is the free-space wave impedance and  $R_r^{P,A}$  is the radiation resistance of the patch

$$R_r^{P,A} = \frac{Q_r}{C_{st} 2\pi f_1}. \quad (6)$$

$C_{st}$  is the total static capacitance [31], and  $Q_r$  the quality factor due to radiation loss [31],[32] p. 186].

The impedance of the loading slots ( $Z_S^P$  and  $Z_S^A$ ) is derived as the parallel combination of three short slots: two identical ones ( $Z_S^V$ ) for the two vertical arms of the U shape, and  $Z_S^H$  for the central part of the slot

$$Z_S^{P,A} = R_S^{P,A} + jX_S^{P,A} = \frac{Z_S^V Z_S^H}{Z_S^V + 2Z_S^H}. \quad (7)$$

$Z_S^V$  and  $Z_S^H$  are derived in Appendix A.

Finally, the equivalent model of the T-junction ( $L_v$ ,  $C_h$ ,  $L_v$ ) is given by [28]

$$L_v = \frac{\mu_0 h}{2\pi} \ln \left( \frac{2c}{\pi C d_v \sqrt{\epsilon_{r,sub}} f_1} \right), \quad (8)$$

$$C_h = \epsilon_0 \epsilon_{r,sub} 2\pi \frac{h_g}{\ln \left( \frac{d_h}{d_v} \right)}, \quad (9)$$

where  $h$  is the thickness of the substrate,  $C$  the Euler's constant,  $\mu_0$  the magnetic permeability of free space,  $d_v$  the diameter of the metallized via,  $d_h$  the diameter of the opening in the ground plane, and  $h_g$  is the thickness of the ground plane (18  $\mu\text{m}$ ).

TABLE II  
VALUES OF THE LUMPED ELEMENTS AT 10 GHz

Passive patch		Active patch		Via hole	
$C_p^P$	12.0 pF	$C_p^A$	11.3 pF	$L_v$	1.18 nH
$L_p^P$	22.2 pH	$L_p^A$	23.8 pH	$C_m$	7.78 fF
$R_p^P$	433 $\Omega$	$R_p^A$	465 $\Omega$		
$R_r^P$	75.3 $\Omega$	$R_r^A$	77.1 $\Omega$		
$R_s^P$	0.26 $\Omega$	$R_s^A$	0.25 $\Omega$		
$C_s^P$	0.19 pF	$C_s^A$	0.20 pF		

#### D. Numerical results

Table II summarizes the lumped element values obtained at 10 GHz with the model described above. The theoretical values of  $C_s^P$  and  $C_s^A$  equal 0.18 pF. They have been optimized ( $C_s^P = 0.19$  pF,  $C_s^A = 0.20$  pF) in order to have a better fit between theoretical and simulated S-parameters. This variation is attributed to the finiteness of the patch and the presence of the ground plane which is not taken into account in the slot model (Appendix A), as well as the two bias lines not accounted for either. The values of the two patch models are slightly different because of the thickness and dielectric constant of the bonding film under the active patch

Full-wave simulations have been also performed with Ansoft HFSS v.12 for both phase states ( $0^\circ$  and  $180^\circ$ ) of the unit-cell. The cell is illuminated by a plane wave under normal incidence. Periodic boundary conditions are applied on four of the boundaries defining the computational domain. In these

simulations, the PIN diodes are represented as lumped  $RLC$  elements ( $R_s = 3.6 \Omega$ ,  $L_d = 0.05$  nH for the *on*-state diode (Fig. 2b), and  $C_t = 42$  fF,  $R_p = 300$  k $\Omega$  for the *off*-state diode (Fig. 2c)), and a block of GaAs material ( $0.68 \times 0.36 \times 0.19$  mm<sup>3</sup> [24],  $\epsilon_r = 12.9$ ).

The theoretical amplitude and phase of the reflection ( $S_{11}$ ) and transmission ( $S_{21}$ ) coefficients are compared in Fig. 5. A good agreement is obtained between the equivalent lumped-element model and the full-wave simulations. The simulated insertion loss is 1.88 dB at 9.75 GHz, and the 3-dB transmission bandwidth spans from 8.88 GHz to 10.35 GHz (14.7%). As shown in Fig. 5a, the simulated  $S_{11}$  and  $S_{21}$  are slightly different in the two states; this small difference is attributed to the asymmetry of the passive patch and the weak interaction between the active and passive patches through the connection via and the opening in the ground plane. As expected, a  $180^\circ$  transmission phase difference is obtained between the two states. The transmission phase computed with the electrical model is in good agreement with the one simulated for the  $0^\circ$  state; the  $180^\circ$  state is not given by the lumped model of Fig. 4 because this phase state originates from the physical orientation of the patch, which can not be represented as a lumped component.

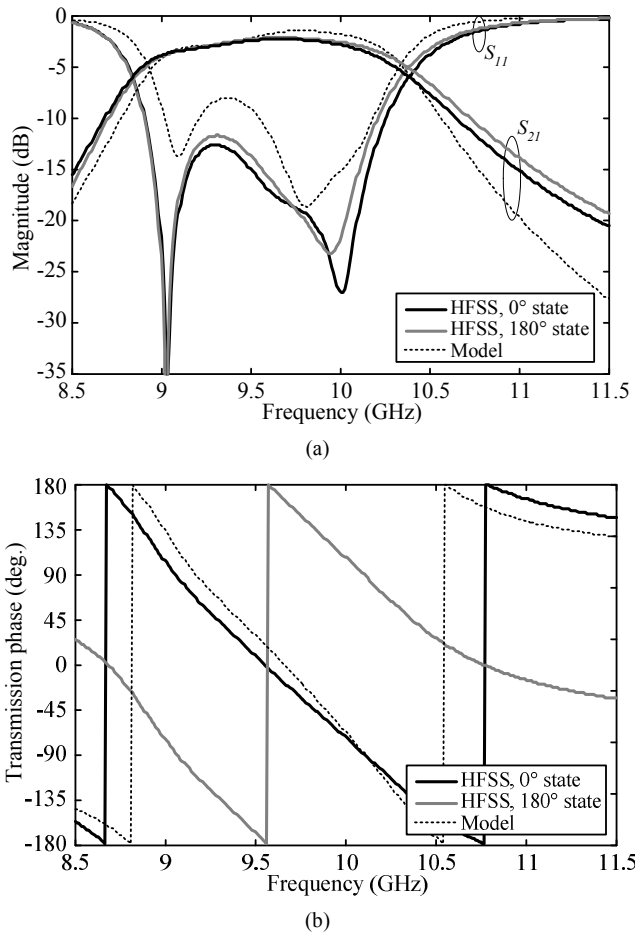


Fig. 5.  $S$ -parameters of the unit-cell obtained from the lumped-element model and the HFSS simulations: (a) magnitude, (b) phase. The lumped-element model is given in Table II. The PIN diode equivalent circuit is the one provided in Section III.A for  $I_{bias} = 10$  mA in the *on* state.

Since a good agreement is obtained between the simulated and modeled  $S$ -parameters, the equivalent circuit model can be

further used to investigate the robustness of the proposed unit-cell with respect to fabrication uncertainties and diode characteristics. To this end, we have performed an exhaustive parametric study of this design. We have found that the most sensitive parameters impacting the frequency response of the unit-cell are the series resistance of the forward-biased diode ( $R_s$ ), the capacitance of the reverse-biased diode ( $C_t$ ), and the connection via diameter ( $d_v$ ).  $R_s$  primarily affects the insertion loss of the unit-cell which varies from 1.16 dB to 1.93 dB for  $R_s = 1$ -4  $\Omega$ . Figs. 6 and 7 represent the  $S$ -parameters for three values of  $C_t$  (30 fF, 42 fF (nominal value), and 65 fF) and three values of  $d_v$  (0.32 mm, 0.38 mm (nominal value) and 0.44 mm). These two parameters have a significant impact on the impedance matching of the unit-cell.

#### IV. EXPERIMENTAL CHARACTERIZATION

The unit-cell has been fabricated (Figs. 8a and 8b) and characterized in an ad-hoc waveguide simulator. In order to guarantee the continuity of the waveguide walls through the prototype, two rings of vias and a large ground plane are used. The measurement setup includes two standard WR-90 waveguides ( $22.86 \times 10.16$  mm<sup>2</sup>) and two ad-hoc rectangular-to-square ( $15 \times 15$  mm<sup>2</sup>) waveguide transitions (Figs. 8c and 8d). In contrast to [33], an ‘incidence’ angle can not be clearly defined in this waveguide measurement set-up because of the tapered rectangular-to-square cross-section on both sides of the unit-cell under test. Instead, the transition length (3.75 mm, i.e.  $\lambda_g/11$  at 10 GHz where  $\lambda_g$  is the guided wavelength for the TE<sub>10</sub> mode in the rectangular waveguide) has been chosen in order to obtain similar  $S$ -parameters as in the ideal case of periodic boundary conditions (PBC) and normal incidence.

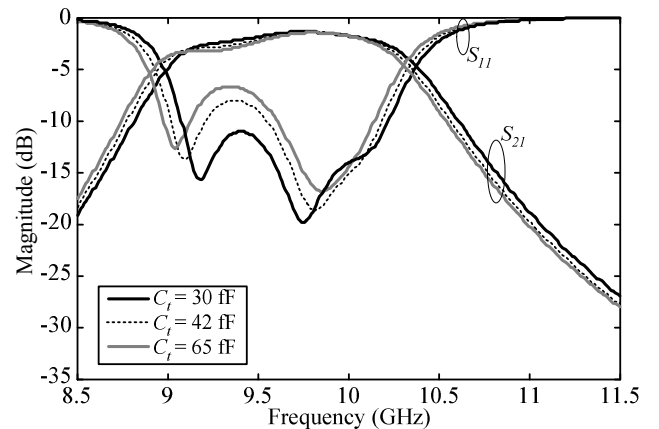


Fig. 6. Influence of the diode reverse capacitance on the  $S$ -parameters of the unit-cell. The lumped-element model is given by Table II. The PIN diode equivalent circuit is the one provided in Section III.A for  $I_{bias} = 10$  mA for the *on* state and  $C_t = 30$ -65 fF for the *off* state.

##### A. Frequency response

The  $S$ -parameters of the unit-cell have been measured between 8.5 and 11.5 GHz. The experimental set-up has been calibrated using a TRL two-port (Through-Reflect-Line) procedure with the reference planes defined at the output of the waveguides (the two transitions are not included in the calibration). The forward bias current equals 10 mA. The experimental frequency response is represented in Fig. 9. As

expected, the measured  $S_{11}$  and  $S_{21}$  coefficients are very similar in both states; the minimum insertion loss equals 1.9 and 1.7 dB at 9.8 GHz in the  $0^\circ$  and  $180^\circ$  phase state, respectively. The 3-dB transmission bandwidth is equal to 1.5 GHz (15% at 10 GHz). The difference between the measured transmission coefficients in both states is less than 0.4 dB in the transmission band. Two different HFSS result series are also shown in Fig. 9: the first one was obtained using PBC and Floquet ports, as explained in Section III.D; in the second one, the complete measurement set-up is simulated (waveguides, transitions, and unit-cell). As one can see, both simulations are in good agreement with the experimental data, and the full simulation model is even in better agreement with the experimental data. Table III compares the experimental values of the insertion loss for both phase states as a function of biasing current. It highlights the trade-off to be made between power consumption and insertion loss. The lowest losses (1.58-1.76 dB) are obtained for a bias current of 20 mA, which would lead to large power consumption. The bias current can be reduced by a factor of 2 (10 mA) or 4 (5 mA) at the expense of 0.1 dB or 0.3 dB of additional losses, respectively.

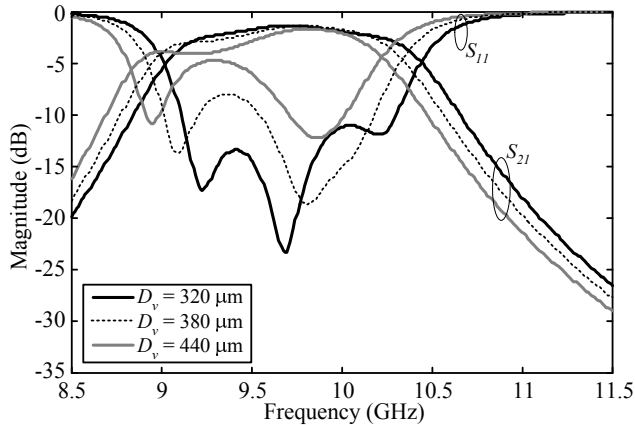


Fig. 7. Influence of the via hole diameter on the  $S$ -parameters of the unit-cell ( $I_{bias} = 10$  mA for the *on*-state diode,  $C_t = 42$  fF for the *off*-state diode). The lumped-element model is given by Table II for  $d_v = 380$   $\mu\text{m}$ . For  $d_v = 320$   $\mu\text{m}$ , the new values of  $L_v$  (Eqn. (8)) and  $C_m$  (Eqn. (9)) are 1.22 nH and 5.65 fF, respectively. For  $d_v = 440$   $\mu\text{m}$ ,  $L_v = 1.13$  nH and  $C_m = 11.4$  fF.

Finally, the computed and measured differential phase response is represented in Fig. 10. Here again, the experimental results are very satisfactory since the maximum phase deviation is less than  $13^\circ$  (compared to the ideal value  $180^\circ$ ) between 8.5 GHz and 11.5 GHz.

TABLE III  
 MEASURED INSERTION LOSS AT 9.75 GHz

Bias current (mA)	Unit-Cell $0^\circ$	Unit-Cell $180^\circ$
	Insertion loss (dB)	Insertion loss (dB)
20	1.76	1.58
10	1.87	1.68
5	2.08	1.86
3	2.33	2.08
2	2.6	2.34
1	3.34	3.04

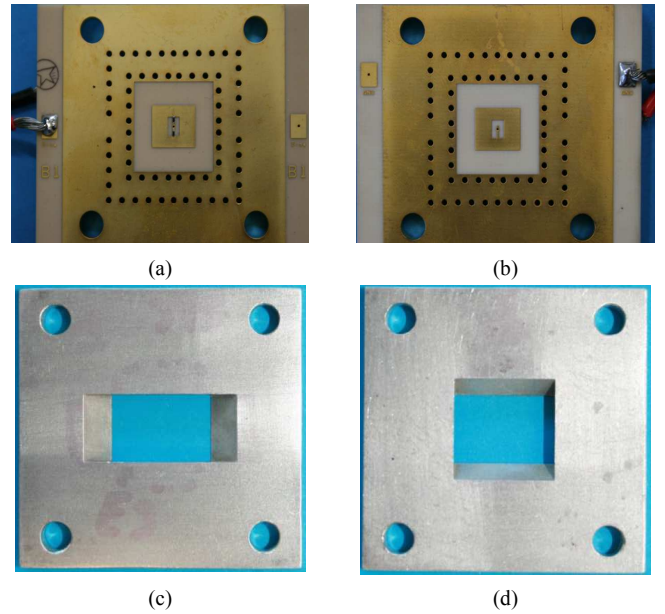


Fig. 8. (a,b) Photographs of the unit-cell prototype: active patch side (a) and passive patch side (b). (c,d) Photographs of the rectangular-to-square waveguide transition: WR-90 waveguide side (c) and unit-cell side (d). The E-plane is vertical in all these photographs.

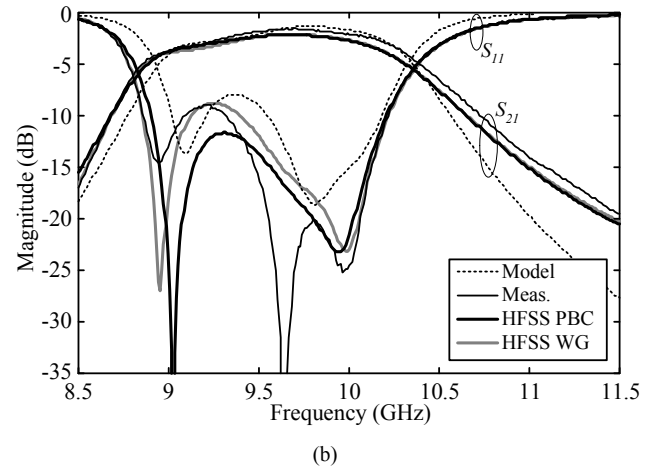
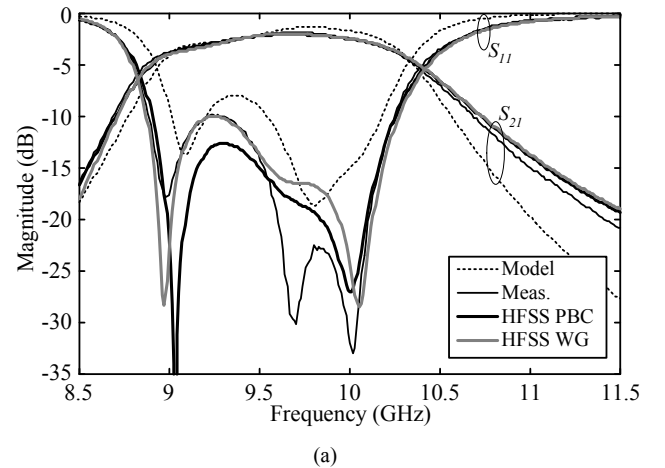


Fig. 9. Measured, analytical (electrical model) and simulated (HFSS)  $S$ -parameters of the unit-cell in the  $0^\circ$  state (a) and  $180^\circ$  state (b). Simulations were performed both with periodic boundary conditions (PBC) and using the complete measurement system (WG).

### B. 1-dB compression point

As this unit-cell is intended to be used in transmit-array applications, it is important to estimate the maximum input power that can be delivered by the primary source to ensure a linear response of the array. To this end, we have measured the 1-dB compression point of the unit-cell. The experimental set-up is represented in Fig. 11a. Several intermediate measurements were performed to determine the characteristics of each block (amplifier gain, waveguide and cable losses) and extract the effective incident power  $P_{in}$  on the unit-cell. The 1-dB compression point of the unit-cell was found to be lower if the diodes are on the side of the incident wave (Diode IN) than if they are on the side of the outgoing wave (Diode OUT); indeed, in the latter case, part of the incident power is reflected or absorbed as losses in the passive patch antenna before reaching the diodes.

The transmission coefficient has been measured in both phase states for a forward-bias current ranging between 2 mA and 20 mA. The results obtained for the  $0^\circ$  phase state at 9.75 GHz, when the incident power illuminates the active patch (Diode IN), are represented in Fig. 11b as a function of  $P_{in}$ . It shows that the 1-dB compression point ( $P_{in}^{1-dB}$ ) varies between 15.2 dBm ( $I_{bias} = 20$  mA) and 14.6 dBm ( $I_{bias} = 2$  mA). In Fig. 11c, the 1-dB compression point is plotted as function of frequency for both phase states, and both orientations of the unit-cell. It exhibits a significant variation as a function of frequency. The two orientations result in a compression point difference of 1-2 dB, corresponding roughly to the insertion losses.

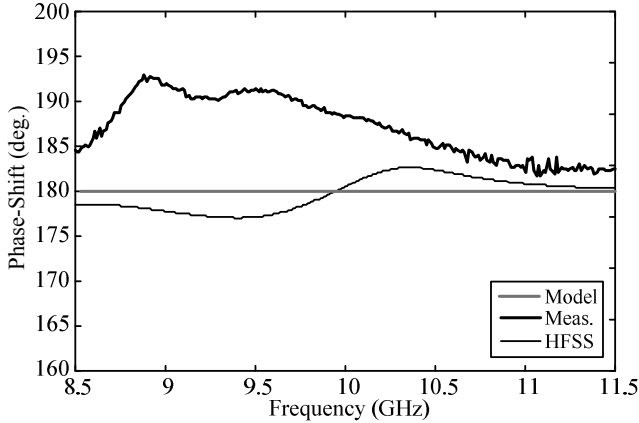


Fig. 10. Measured and simulated (electrical model and HFSS) differential phase-shift between both phase states of the unit-cell.

From these results, it is interesting to evaluate a lower bound of the maximum transmission power for a typical transmit-array based on this unit-cell. The power radiated by the focal source  $P_{FS}$  and the incident power impinging on the central cell  $P_c$  of the transmit-array are related by

$$P_{FS} = \frac{4\pi F^2}{G_{FS} A_{phy}} P_c, \quad (10)$$

where  $F$  is the focal distance,  $G_{FS}$  is the gain of the focal source, and  $A_{phy}$  is the area of the unit-cell. If we consider, as an example, the X-band transmit-array designed in our previous work [15] ( $F = 260$  mm,  $G_{FS} = 10$  dBi,  $20 \times 20$  elements), the maximum power that can be transmitted by the

focal source to guarantee a linear operation of the array is around 41 dBm (12.5 W) for a bias current of 20 mA and 40 dBm (10 W) for a bias current of 2 mA in case of Diode IN orientation and around 42 dBm (16 W) for a bias current between 2-20 mA in the case of Diodes OUT orientation. As this evaluation is performed for the compression limit of the central unit-cell ( $P_c = P_{in}^{1-dB}$ ) and as the other unit-cells of the array receive a lower incident power, the actual compression point of the transmit-array is expected to be higher than the values mentioned above.

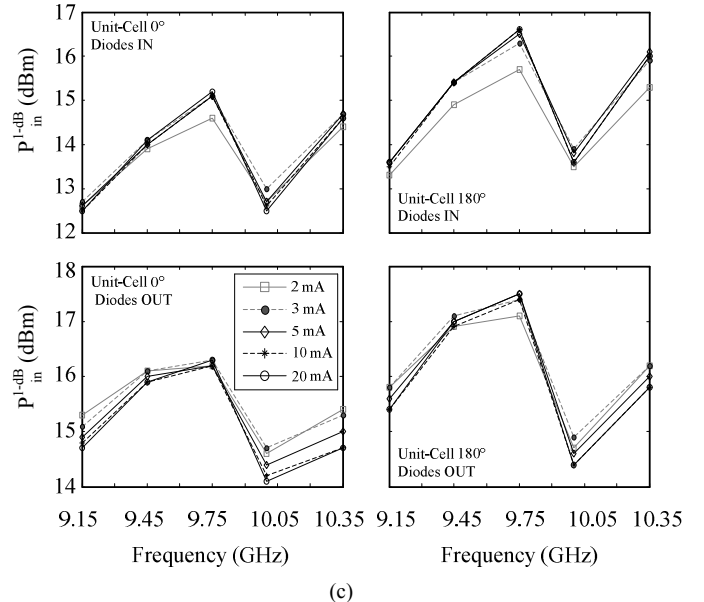
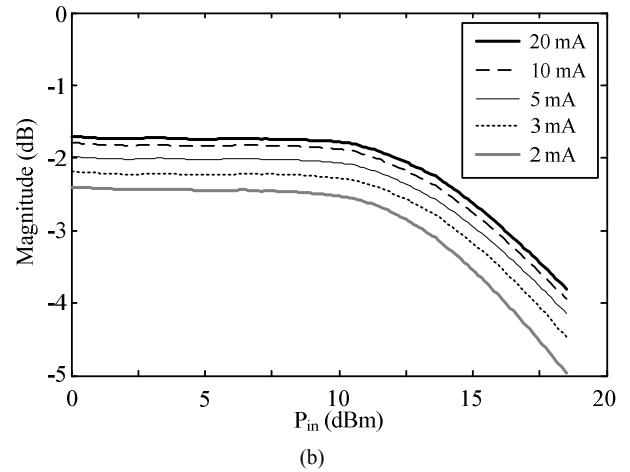
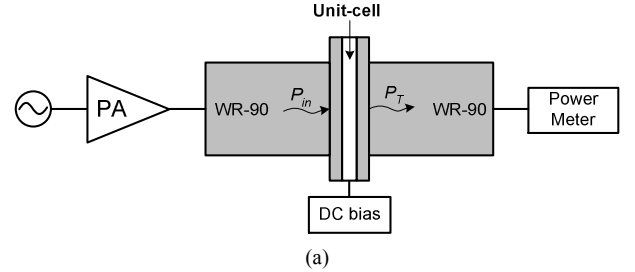


Fig. 11. 1-dB compression point of the unit-cell. (a) Measurement setup. (b) Transmission coefficient at 9.75 GHz as a function of the incident power  $P_{in}$  for several values of the forward bias current ( $0^\circ$  state). (c) 1-dB compression point as a function of frequency for both phase states and both orientations.

Diodes IN: diodes on the side of the incident wave, Diodes OUT: diodes on the side of the outgoing wave.

### C. Measurement of the unit-cell radiation pattern

The radiation patterns of the unit-cell have been measured in far-field for both states. The gain was determined with a 10-dBi standard gain horn antenna. The unit-cell has been mounted at the end of a WR-90 waveguide using the same rectangular-to-square waveguide transition as in Figs. 8c-d. The second face of the unit-cell is left open so that its radiation pattern can be measured. Fig. 12 represents (i) the gain radiation pattern measured at 9.75 GHz in the two principal planes for the  $0^\circ$ -state and (ii) the differential phase-shift between the two states. The unit-cell exhibits a gain of 5 dBi at broadside ( $\theta = 0^\circ$ ); it is in good agreement with the simulations performed in the same configuration (waveguide feed on one side of the unit-cell and free-space on the other side). The small asymmetry observed on the radiation pattern measured in E-plane is very likely due to the fabrication uncertainties such as the position of the central via being slightly off-centered and the position of the PIN diodes not perfectly symmetrical. The gain radiation patterns obtained in the  $180^\circ$  phase state are nearly identical (the gain difference is lower than 0.1 dBi), which will guarantee a good amplitude distribution across a transmit-array based on the proposed unit-cell.

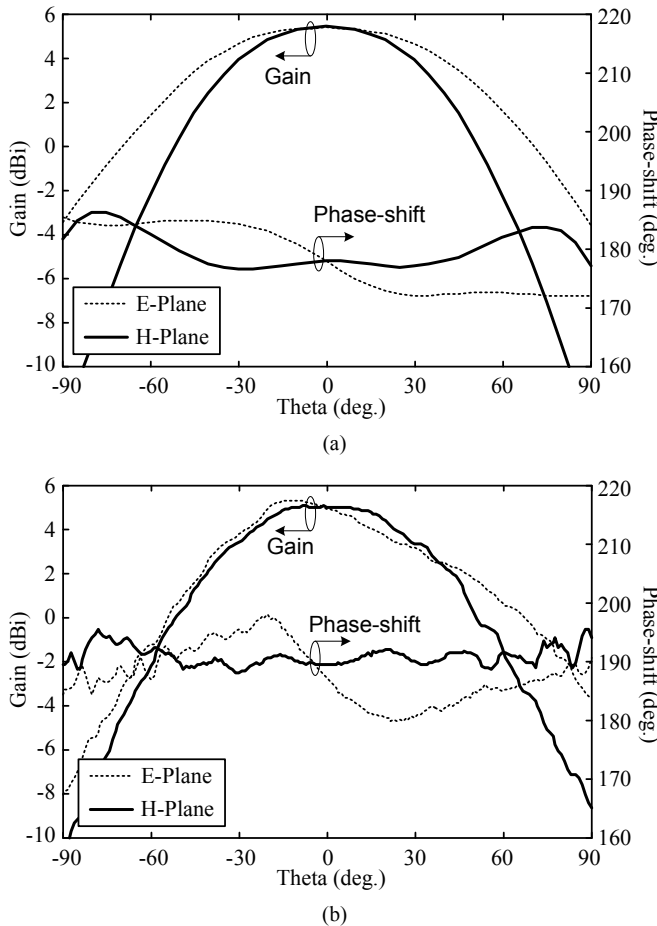


Fig. 12. Simulated (HFSS) (a) and measured (b) gain radiation pattern ( $0^\circ$  state) and differential phase-shift of the reconfigurable unit-cell at 9.75 GHz ( $I_{bias} = 10$  mA).

It is important to note that the actual radiation gain of the unit-cell in the array environment will be slightly different than the one measured in this experiment, due to the surrounding unit-cells. Simulations using periodic boundary conditions to mimic an infinite array indicate a theoretical gain of 4.7 dBi and 3.8 dBi for the passive and active patch respectively.

## V. CONCLUSION

An electronically reconfigurable unit-cell with two phase states has been presented for linear-polarization transmit-arrays in X-band. It consists of two slot-loaded rectangular patch antennas (passive and active patch) connected by a metallized via. The phase response is controlled by activating two PIN diodes integrated on the active patch.

The proposed design has been modeled with a lumped-element circuit derived from analytic formulas and further optimized with full-wave simulations. To validate the numerical results, a prototype has been manufactured and tested in an ad-hoc waveguide simulator. The characterizations include the frequency response, the power response and the radiation pattern. A good agreement has been obtained between the analytical model, the full-wave simulations and measurements.

The main advantages of this unit-cell are its wide transmission bandwidth with constant phase-shift, and its low insertion losses nearly independent of the phase state.

## VI. ACKNOWLEDGMENT

This work has been partly funded by the Direction Générale de l'Armement (DGA/DS/MRIS), France.

## APPENDIX A

### VERTICAL AND HORIZONTAL SLOTS IMPEDANCE

In Section III.C, the complex impedance  $Z_S^{P,A}$  of the U-slot is defined as the parallel combination of two vertical slots and a horizontal one (Eqn. 7). Their impedances are labeled  $Z_S^V$  and  $Z_S^H$ , respectively.

The Booker's extension of the Babinet's principle [30] shows that it is possible to calculate the self impedance of a slot etched in a large ground plane using the duality principle with an electric dipole. As explained in [34], the presence of a dielectric substrate (of permittivity  $\epsilon_r$ ) close to the slot can be taken into account in the dual problem by a magnetic substrate with a permeability  $\mu_r = \epsilon_r$  close to the dielectric dipole. Based on this principle, the slot impedances  $Z_S^V$  and  $Z_S^H$  in Eqn. (7) are estimated by

$$Z_S^{V,H} = \frac{\eta^2}{4Z_d^{V,H}}, \quad (11)$$

where  $\eta$  is the wave impedance of the magnetic substrate and  $Z_d^{V,H} = R_d^{V,H} + jX_d^{V,H}$  is the impedance of the (dual) electric dipoles.

For a thick dipole antenna, i.e. a dipole whose width can not be considered much smaller than its length, an approximated

expression of the self impedance is proposed in [35] where the current distribution along the dipole is the same as along a lossy transmission-line

$$R_d^{V,H} = \frac{\eta_0}{\pi} \left[ \ln \left( \frac{L_{s,h}}{t} \right) - 1 \right] \frac{\sinh(\alpha L_{s,h}) - \frac{\alpha c}{2\pi f_2} \sin \left( \frac{2\pi f_2}{c} L_{s,h} \right)}{\cosh(\alpha L_{s,h}) - \cos \left( \frac{2\pi f_2}{c} L_{s,h} \right)} \quad (12a)$$

$$X_d^{V,H} = -\frac{\eta_0}{\pi} \left[ \ln \left( \frac{L_{s,h}}{t} \right) - 1 \right] \frac{\frac{c\alpha}{2\pi f_2} \sinh(\alpha L_{s,h}) + \sin \left( \frac{2\pi f_2}{c} L_{s,h} \right)}{\cosh(\alpha L_{s,h}) - \cos \left( \frac{2\pi f_2}{c} L_{s,h} \right)}, \quad (12b)$$

$$\alpha = \frac{\left( \frac{\pi f_2}{c} L_{s,h} \right)^2}{2L_{s,h} \left[ \ln \left( \frac{L_{s,h}}{t} \right) - 1 \right]}, \quad (12c)$$

where  $L_h = W_s - 2t$ , and  $L_s$  is the length of the vertical arms of the slots (Fig. 1b). Eqns. (12a)-(12c) are used to compute  $Z_S^{P,A}$  in Eqn. (7).

#### REFERENCES

- [1] W. Menzel, "Millimeter-wave radar for civil applications," *Proceedings of the 7th European Radar Conference (EuMW 2010)*, Paris, France, 30 Sep.-1 Oct. 2010.
- [2] M. Ettore, R. Sauleau, L. Le Coq, and F. Bodereau, "Single-folded leaky-wave antennas for automotive radars at 77 GHz," *IEEE Antennas Propag. Lett.*, vol. 9, pp. 858–862, 2010.
- [3] S.-Q. Xiao, M.-T. Zhou, and Y. Zhang, "Millimeter wave technology in wireless PAN, LAN, and MAN," *CRC Press*, 2008.
- [4] P. Smulders, "Exploiting the 60 GHz band for local wireless multimedia access: prospects and future directions," *IEEE Commun. Mag.*, Jan. 2002.
- [5] L. Schwartzman and L. Topper, "Analysis of phased array lenses," *IEEE Trans. Antennas Propag.*, vol. 16, no. 6, pp. 628–632, Nov. 1986.
- [6] D. T. McGrath, "Planar three-dimensional constrained lenses," *IEEE Trans. Antennas Propag.*, vol. 34, no. 6, pp. 46–50, Jun. 1986.
- [7] D. M. Pozar, "Flat lens antenna concept using aperture coupled microstrip patch," *Elec. Letters*, vol. 32, no. 23, pp. 2109–2111, Nov. 1996.
- [8] H. Kaouach, L. Dussopt, J. Lantéri, R. Sauleau, and Th. Koleck, "Wideband low-loss linear and circular polarization transmit-array in V-band," *IEEE Trans. Antennas Propag.*, accepted for publication.
- [9] A. Abbaspour-Tamijani, K. Sarabandi, and G. M. Rebeiz, "A millimeter-wave bandpass filter-lens array," *IET Microwaves Antennas and Propag.*, vol. 1, no. 2, pp. 388–395, Apr. 2007.
- [10] R. Sauleau and B. Barès, "A complete procedure for the design and optimization of arbitrarily-shaped integrated lens antennas," *IEEE Trans. Antennas Propag.*, vol. 54, no. 4, pp. 1122–1133, Apr. 2006.
- [11] J. R. Costa, C. A. Fernandes, G. Godi, R. Sauleau, L. Le Coq, and H. Legay, "Compact Ka-band lens antennas for LEO satellites," *IEEE Trans. Antennas Propag.*, vol. 56, no. 5, pp. 1251–1258, May 2008.
- [12] A.V. Boriskin, R. Sauleau, and A.I. Nosich, "Performance of hemielliptic dielectric lens antennas with optimal edge illumination," *IEEE Trans. Antennas Propag.*, vol. 57, no. 7, pp. 2193–2198, Jul. 2009.
- [13] R. A. York and Z. Popovic, "Active and quasi-optical arrays for solidstate power combining," *New York: Wiley*, 1997.
- [14] Z. Popovic and A. Mortazawi, "Quasi-optical transmit/receive front ends," *IEEE Trans. Microw. Theory Tech.*, vol. 46, no. 11, pp. 1964–1975, Nov. 1998.
- [15] H. Kaouach, L. Dussopt, R. Sauleau, and Th. Koleck, "X-band transmit-arrays with linear and circular polarization," *4th European Conference Antennas Propag. (EuCAP 2010)*, Barcelona, Spain, 12–16 Apr. 2010.
- [16] M. B. Perotoni, S. Rondineau, R. Lee, D. Consonni, and Z. Popovic, "X-band discrete lens array for a satellite communication ground station antenna," *2005 SBMO/IEEE MTT-S Int. Conf. Microwave and Optoelectronics*, pp. 197–200, 25–28 Jul. 2005.
- [17] B. Wu, A. Suntiyo, M. E. Potter, and M. Okoniewski, "On the selection of the number of bits to control a dynamic MEMS reflectarray," *IEEE Antenna Wireless Propag. Letters*, vol. 7, pp. 183–186, 2008.
- [18] J. Y. Lau and S. V. Hum, "A planar reconfigurable aperture with lens and reflectarray modes operation," *IEEE Trans. Antennas Propag.*, vol. 58, no. 12, pp. 3547–3555, Dec. 2010.
- [19] P. Padilla de la Torre, A. Muñoz-Acevedo, M. Sierra-Castañer, and M. Sierra-Pérez, "Electronically reconfigurable transmitarray at Ku-band for microwave applications," *IEEE Trans. Antennas Propag.*, vol. 58, no. 8, pp. 2571–2579, Aug. 2010.
- [20] C.-C. Cheng, B. Lakshminarayanan, and A. Abbaspour-Tamijani, "A programmable lens-array antenna with monolithically integrated MEMS switches," *IEEE Trans. Microwaves Theory Tech.*, vol. 57, no. 8, pp. 1874–1884, Aug. 2009.
- [21] S. Montori, C. Fritzsche, L. Marcaccioli, R. V. Gatti, R. Jakoby, and R. Sorrentino, "Design and measurement of a 1-bit reconfigurable elementary cell for large electronic steerable reflectarrays," *40th European Microwave Conference (EuMc 2010)*, Paris, France, 28–30 Sep., 2010.
- [22] H. Kamoda, T. Iwasaki, J. Tsumochi, T. Kuku, and O. Hashimoto, "60-GHz electrically reconfigurable large reflectarray using single-bit phase shifter," *IEEE Trans. Antennas Propag.*, vol. 59, no. 7, pp. 2524–2531, Jul. 2011.
- [23] A. Clemente, L. Dussopt, R. Sauleau, P. Potier, and P. Pouliguen, "1-bit reconfigurable unit-cell for transmit-array applications in X-band," *IEEE Antennas and Propag. Soc. Int. Symp.*, Spokane (WA), pp. 684–687, Jul. 2011.
- [24] MA-COM Technology Solutions, MA4AGP907 and MA4AGFCP910 AlGaAs Flip Chip PIN Diodes [Online]. Available: [www.macomtech.com/datasheets/MA4AGP907\\_FCP910.pdf](http://www.macomtech.com/datasheets/MA4AGP907_FCP910.pdf).
- [25] The PIN diode circuit designers' handbook [Online]. Available: <http://www.microsemi.com/idx.asp?MN=435>.
- [26] K. F. Lee, S. L. S. Yang, A. A. Kishk, and K. M. Luk, "The versatile U-slot patch antenna," *IEEE Antennas Propag. Mag.*, vol. 52, no. 1, pp. 71–88, Feb. 2010.
- [27] R. Bhalla and L. Shafai, "Resonance behavior of single U-slot microstrip patch antenna," *Microw. Optical Tech. Lett.*, vol. 32, no. 5, pp. 33–335, Mar. 2002.
- [28] R. Garg, P. Bhartia, I. Bahl, and A. Ittipiboon, "Microstrip antenna design handbook," *Artech House*, Boston, MA, 2001.
- [29] W. Richards, Y. T. Lo, and D. Harrison, "An improved theory for microstrip antennas and applications," *IEEE Trans. Antennas Propag.*, vol. 29, no. 1, pp. 38–46, Jan. 1981.
- [30] C. A. Balanis, "Antenna theory: analysis and design," 3rd edition, *Wiley Interscience*, 2005.
- [31] M. Kara, "An efficient technique for the computation of the rectangular microstrip antenna elements with thick substrate," *Microw. Optical Tech. Lett.*, vol. 13, no. 6, pp. 363–369, Dec. 1996.
- [32] C. A. Balanis, "Modern antenna handbook," *Wiley Interscience*, 2008.
- [33] P. W. Hannan and M. A. Balfour, "Simulation of phased array in waveguide," *IEEE Trans. Antennas Propag.*, vol. 13, no. 3, pp. 342–353, May 1965.
- [34] B. D. Papović and A. Nešić, "Some extensions of the concept of complementary electromagnetic structures," *IEE Proc. Microwaves, Antennas and Propag.*, vol. 132, no. 2, pp. 131–137, Apr. 1985.
- [35] G. Dubost, "Flat radiating dipoles and applications to arrays," *Research Studies Press*, Chichester, England, 1981.



**Antonio Clemente** received the B.S. and M.S. degree in telecommunication engineering and remote sensing systems from the University of Siena, Siena, Italy, in 2006 and 2009. From October 2008 to May 2009 he realized his master thesis project at Technical University of Denmark (DTU), Lyngby, Denmark, where he worked on spherical near-field antenna measurements. Since October 2009, he has been a Ph.D. student in signal processing and telecommunication systems at University of Rennes 1, France and a research assistant at CEA-LETI, Grenoble, France. His research interests include quasi-optic reconfigurable antennas at microwave and millimeter-wave frequencies.



**Laurent Dussopt** (S'00–A'01–M'03–SM'07) received the M.S. and Agrégation degrees in electrical engineering from the Ecole Normale Supérieure de Cachan, France, in 1994 and 1995, the Ph.D. degree in electrical engineering from the University of Nice-Sophia Antipolis, France, in 2000, and the “Habilitation à Diriger des Recherches” degree from the University Joseph Fourier, Grenoble, France, in 2008.

From September 2000 to October 2002, he was a Research Fellow with The University of Michigan at Ann Arbor. Since 2003, he is a Research Engineer at CEA-LETI, Grenoble, France. His research interests include reconfigurable antennas, millimetre-wave integrated antennas and antenna arrays, RF-MEMS devices and systems.

Dr. Dussopt received the Lavoisier Postdoctoral Fellowship from the French government in 2000 and was a co-recipient of the 2002 Best Student Paper Award (Second Prize) presented at the IEEE Radio Frequency Integrated Circuit (RFIC) Conference.



**Ronan Sauleau** (M'04–SM'06) graduated in electrical engineering and radio communications from the Institut National des Sciences Appliquées, Rennes, France, in 1995. He received the Agrégation degree from the Ecole Normale Supérieure de Cachan, France, in 1996, and the Doctoral degree in signal processing and telecommunications and the “Habilitation à Diriger des Recherche” degree from the University of Rennes 1, France, in 1999 and 2005, respectively.

He was an Assistant Professor and Associate Professor at the University of Rennes 1, between September 2000 and November 2005, and between December 2005 and October 2009. He has been a full Professor in the same University since November 2009. His current research fields are numerical modelling (mainly FDTD), millimeter-wave printed and reconfigurable (MEMS) antennas, lens-based focusing devices, periodic and non-periodic structures (electromagnetic bandgap materials, metamaterials, reflectarrays, and transmitarrays) and biological effects of millimeter waves. He has received seven patents and is the author or coauthor of more than 100 journal papers and more than 240 publications in international conferences. Prof. Sauleau received the 2004 ISAP Conference Young Researcher Scientist Fellowship (Japan) and the first Young Researcher Prize in Brittany, France, in 2001 for his research work on gain-enhanced Fabry-Perot antennas. In September 2007, he was elevated to Junior member of the “Institut Universitaire de France”. He was awarded the Bronze medal by CNRS in 2008.

#### **Patrick Potier**

**Pilippe Pouliguen** was born in Rennes, France, on 1963. He received the M.S. degree in signal processing and telecommunications and the Ph.D. degree from the University of Rennes 1, France, in 1986 and 1990 respectively.

In 1990, he joined the Direction Générale de l'Armement (DGA) at the Centre d'Electronique de l'Armement (CELAR), in Bruz, France, where he was a “DGA expert” in electromagnetic radiation and radar signatures analysis. He was also in charge of the EMC (Expertise and ElectroMagnetism Computation) laboratory of CELAR. Now, he is the head of acoustic and radio-electric waves domain at the office for advanced research and innovation of the strategy directorate, DGA, France. His research interests include electromagnetic scattering and diffraction, Radar Cross Section (RCS) measurement and modeling, asymptotic high frequency methods, radar signal processing and analysis, antenna scattering problems and Electronic Band Gap Materials.

In these fields, he has published more than 30 articles in refereed journals and more than 80 conference papers.